

## Anomalous KCl(001) Surface Corrugation from Fast He Diffraction at Very Grazing Incidence

G. A. Bocan<sup>1,\*</sup>, H. Breiss<sup>2</sup>, S. Szilasi<sup>2</sup>, A. Momeni<sup>2,3</sup>, E. M. Staicu Casagrande<sup>2</sup>,  
M. S. Gravielle<sup>4</sup>, E. A. Sánchez<sup>1</sup>, and H. Khemliche<sup>2</sup>

<sup>1</sup>*Instituto de Nanociencia y Nanotecnología, Nodo Bariloche (CONICET-CNEA) and Instituto Balseiro (U. N. Cuyo),  
Centro Atómico Bariloche, Avenida Bustillo 9500, 8400 San Carlos de Bariloche, Argentina*

<sup>2</sup>*Université Paris-Saclay, CNRS, Institut des Sciences Moléculaires d'Orsay, 91405 Orsay, France*

<sup>3</sup>*CY Cergy Paris Université, F-95000 Cergy, France*

<sup>4</sup>*Instituto de Astronomía y Física del Espacio (UBA-CONICET),  
Casilla de Correo 67, Sucursal 28, C1428EGA Buenos Aires, Argentina*



(Received 20 December 2019; accepted 31 July 2020; published 28 August 2020)

We present theoretical and experimental evidence of an anomalous surface corrugation behavior in He-KCl(001) for incidence along  $\langle 110 \rangle$ . When the He normal energy decreases below 100 meV, i.e., He-surface distances  $Z > 2 \text{ \AA}$ , the corrugation unexpectedly increases up to an impressive  $\gtrsim 85\%$ . This is not due to van der Waals interactions but to the combination of soft potential effects and the evolution of He-cation and He-anion interactions with  $Z$ . This feature, not previously analyzed on alkali-halide surfaces, may favor the alignment properties of weakly interacting overlayers.

DOI: [10.1103/PhysRevLett.125.096101](https://doi.org/10.1103/PhysRevLett.125.096101)

The design of promising new materials in the form of thin film stacks brings along the challenge of producing such heterostructures to the highest quality and thus requires an accurate knowledge of the relevant features that rule quasiepitaxial growth. One such feature is the substrate surface corrugation, which has been shown to drive the overlayer-substrate relative orientation even for weakly interacting interfaces, such as organic-inorganic or transition metal dichalcogenides systems [1,2].

Grazing incidence fast atom diffraction (GIFAD) [3,4] is a highly sensitive and nondamaging probe of the projectile-surface interaction potential. Particularly well suited for a thorough exploration of the surface electronic corrugation, it has already provided valuable structural information on a variety of systems [5–11], and its grazing geometry makes it compatible with *in situ* monitoring of thin film growth [12,13].

GIFAD occurs when keV-energy projectiles impinge on a surface along a low-index crystallographic direction, under axial surface channeling conditions [14]. The GIFAD pattern arises from the combination of (a) inter-channel interference, originated from the periodic array of channels, giving the Bragg peaks and (b) intrachannel interference, originated from the corrugation of the interaction potential within a given channel, giving the rainbow peak as well as the supernumerary rainbows [15]. The result on the detection plane is a sequence of Bragg maxima modulated by the underlying intrachannel interference [15,16].

In this Letter we employ GIFAD to investigate the corrugation of the KCl(001) surface when probed with

low normal energy  ${}^4\text{He}^0$  projectiles along the  $\langle 110 \rangle$  channel. We present experimental data, information provided by the potential energy surface (PES) and simulations of the scattering dynamics, all of which put forward a counterintuitive and notorious increase of the surface corrugation with decreasing normal energy  $E_{\perp}$  in the low  $E_{\perp} \lesssim 60 \text{ meV}$  range, i.e., for He-surface distances  $Z > 2.2 \text{ \AA}$ . Although long-distance surface corrugation increases have been experimentally observed by GIFAD for He/LiF(001) ( $\sim 12\%$ ) [17] and He/KBr(001) ( $\sim 45\%$ ) [18], this is, to our knowledge, the first time such an overwhelmingly large ( $\gtrsim 85\%$ ) increase is reported. Furthermore, we prove that the ruling factors of this puzzling feature are the evolution of the He-anion and He-cation interactions with  $Z$  and the continuance of the projectile-surface interaction during the whole scattering process (i.e., soft potential effects, SPE).

The experiments were performed at room temperature in a GIFAD setup similar to that of Ref. [13]. The KCl(001) sample was cleaved in air and immediately transferred to the ultra-high-vacuum chamber. Once mounted on a five-axis manipulator it was prepared *in situ* by annealing at about 650 K to ensure its cleanness and crystallographic order (corroborated from the well-defined GIFAD patterns obtained [19]). The  ${}^4\text{He}^0$  beam was formed by neutralizing a  $\text{He}^+$  beam with primary energies in the 300–600 eV range. Following the neutralization cell, a set of apertures of  $0.4 \times 0.09 \text{ mm}^2$  placed 0.36 m apart were used to reduce the beam divergence to less than 1 mrad. The two-dimensional angular distributions of scattered projectiles were collected by placing a detector formed by a

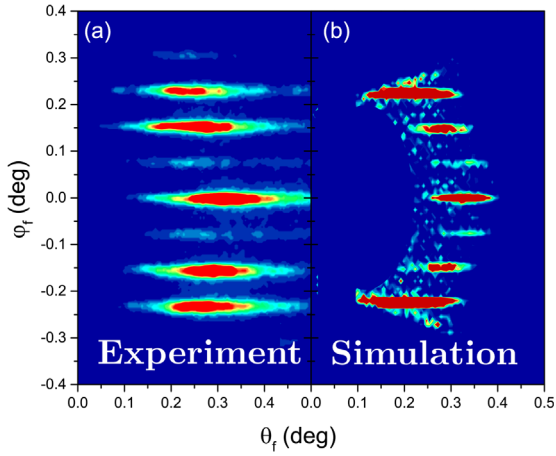


FIG. 1. GIFAD patterns for  ${}^4\text{He} \rightarrow \langle 110 \rangle \text{KCl}(001)$  with incidence energy  $E = 600$  eV and  $E_{\perp} = 0.021$  eV.  $\varphi_f(\theta_f)$ : azimuthal (polar) angular position of the scattered atoms.

microchannel plate, a phosphor-coated screen and a CCD camera in the forward direction at a distance of 1.27 m. In Fig. 1 we depict a GIFAD pattern for 600 eV  ${}^4\text{He}$  atoms with  $E_{\perp} = 21$  meV. The simulated pattern, that shows good accord with the experiment, was obtained with the surface initial value representation (SIVR) [20,21], a well-established semiquantum approach to describe the scattering dynamics [22,23]. Note that collimation [21], surface defects, and thermal vibrations may contribute to the elongation of the Bragg spots along the polar angle, though the latter two are not included in the simulations. Such polar spread does not affect our GIFAD-derived results, based on the elastic contribution to the intensity ( $\theta_f = \theta_i \pm 0.035^\circ$  for the central Bragg order) [19].

The experimental corrugation, presented in Fig. 2(a), was obtained by processing the GIFAD patterns to get the effective interaction potential [7,19,24]. Since low- $E_{\perp}$  scattering takes place far from the surface, it should be ruled by a mild potential landscape, yielding a decreasing surface corrugation with decreasing  $E_{\perp}$  but, intriguingly, we find that the corrugation increases with decreasing  $E_{\perp}$  and this increase gets particularly sharp below 40 meV.

In order to gain more insight into this unexpected behavior we built a high-precision potential energy surface (PES) for the He/KCl(001) system based on density functional theory (DFT), using the Perdew-Burke-Ernzerhof (PBE) exchange-correlation functional [25] (henceforth, the PBE PES, further details in Ref. [22]). When the PES is averaged along the channeling direction ( $\hat{x}$ ), the axial potential  $V^{2D}(Y, Z)$  that actually rules the scattering process [26] is obtained, where  $Y$  is the position across the channeling direction. In Fig. 2(b) we show equipotential curves of the axial PBE PES, from which the *intrinsic* corrugation for a given  $E_{\perp}$  is obtained from the corresponding amplitude  $\Delta Z = Z_{\max} - Z_{\min}$ .

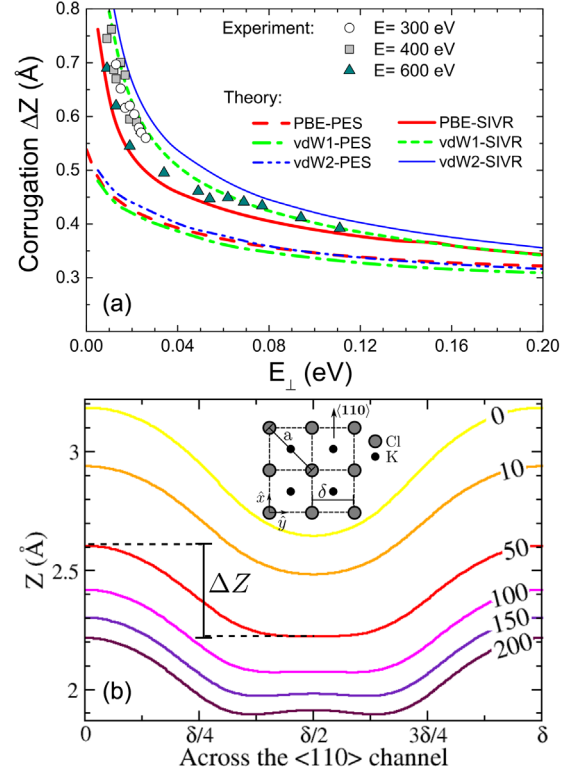


FIG. 2. (a) Surface corrugation for  ${}^4\text{He} \rightarrow \langle 110 \rangle \text{KCl}(001)$  obtained from experiments, the three PESs considered and the respective SIVR simulations. (b) PBE PES equipotential curves for  $0 \leq E_{\perp} \leq 200$  meV. Inset: surface geometry.

Energy regions for which atoms scatter relatively far from the surface ( $Z > 2$  Å) may bring along non-negligible van der Waals (vdW) interactions, left aside in the PBE PES. Hence, we built two additional PESs [19,27], where we replaced the PBE exchange-correlation functional by the rVV10 [28] and the DF2b86r [29] ones (henceforth, respectively, labeled vdW1 and vdW2), which include vdW interactions in a self-consistent fashion though with different approaches. The intrinsic corrugations obtained with the three PESs give very similar curves [see Fig. 2(a)], in good accord with the trend of the experimental values, though about 25% below them. The intrinsic corrugation increase is thus not due to vdW interactions but should rather be explained through a thorough analysis of the axial PBE PES [30].

The equipotential profiles across the  $\langle 110 \rangle$  channel [see inset in Fig. 2(b)] have maxima over the  $\text{Cl}^-$  rows. At midchannel, over the  $\text{K}^+$  row, there is a central minimum for  $E_{\perp} \lesssim 60$  meV and a local maximum for  $E_{\perp} \gtrsim 60$  meV. The latter creates two off-center minima which migrate away from midchannel with increasing  $E_{\perp}$ . The equipotential curves show that the He- $\text{Cl}^-$  interaction (as obtained from DFT calculations) is always more repulsive than the He- $\text{K}^+$  one. The evolution of these interactions upon changing  $E_{\perp}$ , particularly the slow sinking of the

central minimum due to the vanishing He-K<sup>+</sup> interaction, makes  $Z_{\min}$  vary slower than  $Z_{\max}$ , explaining the intrinsic corrugation increase.

The residual discrepancy between the intrinsic and the experimental corrugations remains nevertheless intriguing, leading us to address the rainbow angle [31], a bright peak in the intrachannel contribution at maximal angular deflection [6,14,15,31]. The rainbow angle shows a well-known high sensitivity to the projectile-surface interaction. While the corrugation affects mainly the intensity of the specular region to which only trajectories reflecting in the flattest regions of the axial PES contribute, the rainbow probes the steepest regions of the axial PES. For a given  $E_{\perp}$ , and within a hard-corrugated wall (HCW) approach [32], we determined the PES rainbow from the steepest slope of the corresponding equipotential curve, while the experimental rainbow was obtained from the processing of the GIFAD pattern [7,19,24].

In Fig. 3(a) we show the experimental rainbow angle together with those obtained from the three PESs considered. The increase observed in the experimental rainbow angle for decreasing low  $E_{\perp}$  is analogous to the one obtained for the corrugation. The PESs rainbows show a mild increase, associated with the sinking central peak in

the potential profiles, but they cannot reproduce the experimental rainbow trend for  $E_{\perp} < 100$  meV. The magnitude of the disagreement, once again unrelated to vdW interactions, strikingly contrasts with the fairly good accord discussed for the corrugation.

Extracting information directly from the  $E_{\perp}$  equipotential curves takes into account the projectile-surface interaction only at the turning point (HCW approach), thus neglecting the continuance of the projectile-surface interaction during the rest of the scattering process (i.e., SPE). We hence performed simulations of the scattering dynamics for each PES considered, by means of the semiquantum SIVR approach [20,21] (henceforth labeled PBE SIVR, vdW1 SIVR, and vdW2 SIVR). The simulations were performed considering coherent illumination of a single channel (no interchannel interference) so that the rainbow angle can be directly obtained from the diffracted distribution. Strikingly, the PBE SIVR rainbow reproduces the experiments in the energy range considered with an almost quantitative agreement. Including vdW contributions results in no significant differences, with vdW1 SIVR and vdW2 SIVR running slightly above PBE SIVR.

The notorious difference observed between the PES and the SIVR rainbow angles, combined with the very good SIVR-experiment accord, reveal in a quantitative manner the importance of SPE in central aspects of GIFAD. These dynamical effects are naturally included in both the SIVR and the experimental rainbows (obtained by processing the GIFAD patterns) while the PES ones assume unrealistic broken-line trajectories.

Soft potential effects for the PBE SIVR case can be visualized in Fig. 3(b) where equipotential curves of the axial PES are shown in 1 : 1 scale. For  $3 \lesssim Z \lesssim 5$  Å this plot shows a noteworthy shallow (<7 meV) attractive region, due to polarization and lower-order attractive interactions within the DFT PES, which markedly alters the shape and corrugation of the equipotential curves. For high enough  $E_{\perp}$  this well is inconsequential, but low- $E_{\perp}$  projectiles traversing this region are strongly affected. This is illustrated in Fig. 3(b) for  $E_{\perp} = 15$  meV. Each equipotential curve deviates the trajectory according to the slope at their contact point so that a steeper slope favors  $E_z \rightarrow E_y$  energy conversion. SIVR trajectories deviate from the HCW one upon entering the well region and also during their way out. In the asymptotic condition the projectile-surface interaction fades out and trajectories become linear but not parallel to the HCW trajectory. In the light of this analysis, the difference between the intrinsic and the experimental corrugations could also be due to SPE. Hence, from our SIVR simulations we selected trajectories contributing to the specular intensity. These trajectories are reflected either around the maximum or the minimum of the equipotential, with near-normal incidence and scattering directions. We can compute their SIVR accumulated phase difference [Eq. (10) in Ref. [20]] and obtain an *effective* corrugation

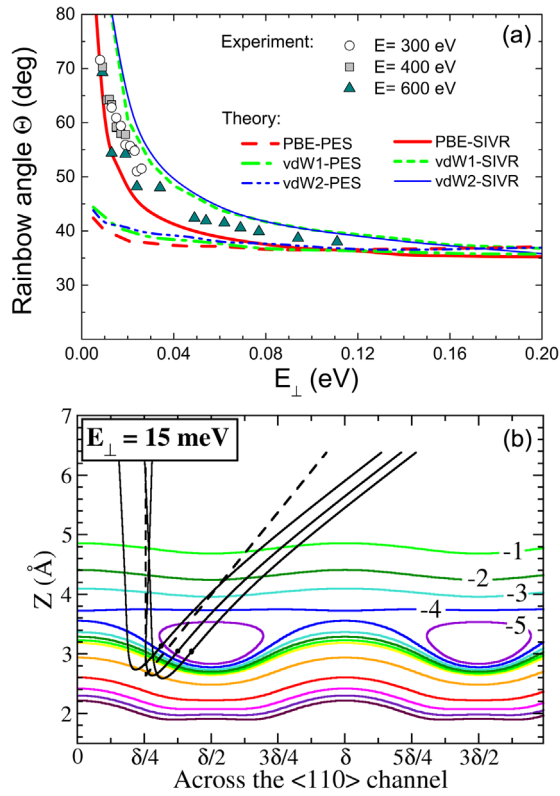


FIG. 3. (a) Rainbow angle for  ${}^4\text{He} \rightarrow \langle 110 \rangle \text{KCl}(001)$ . (b) PBE equipotential curves [only energies (meV) not shown in Fig. 2(b) are labeled] and trajectories contributing to the rainbow intensity (dashed black line: HCW, full black line: SIVR).

from  $\Delta\Phi^{\text{SIVR}} = 2k_{\perp}(\Delta Z)^{\text{SIVR}}$  [depicted in Fig. 2(a)]. The agreement with experiments is remarkable and shows that the PBE SIVR calculation captures the factors determining the corrugation increase. From Fig. 2(a), the differences between the SIVR and PES curves, together with the SIVR-experiment accord, provide a quantitative measure of SPE on the effective experimental corrugation obtained by means of the GIFAD technique.

In summary, we report a counterintuitive increase of the corrugation and the rainbow angle for decreasing low  $E_{\perp}$ , by means of the GIFAD technique, in  ${}^4\text{He-KCl}(001)$  along the  $\langle 110 \rangle$  direction. This increase reaches an overwhelmingly large  $\gtrsim 85\%$  and is independently obtained from experiments and simulations. Its origin, unrelated to vdW effects, lies in the different evolution of He-cation and He-anion interactions, combined with SPE. As the latter do not strongly affect the corrugation dependence on  $E_{\perp}$ , the experimental curve preserves the intrinsic corrugation trend, meaning that GIFAD provides reliable information on this surface feature. In contrast, the rainbow increase is almost fully explained in terms of SPE, strongly enhanced by the shallow well, whose steepest regions markedly deviate low- $E_{\perp}$  rainbow trajectories.

The same two factors are likely responsible for the corrugation increases at low  $E_{\perp}$  reported for He/KBr(001) [18] and He/LiF(001) [17] (and expected for other alkali-halide surfaces) along this same channel. Particularly, for He/LiF, the much less spectacular corrugation increase is probably only due to SPE as the He-Li interaction is far vanished in the energy range considered. Also, we expect SPE to rule a marked rainbow increase feature, given the reported presence of shallow wells [33].

Thin alkali-halide layers (mainly NaCl and LiF) are often used to improve charge injection in organic electronic devices. The enhanced corrugation of KCl(001) at typical physisorption distances may favor the alignment properties of weakly interacting overlayers [1,2], improving their crystalline quality and thus the device performance. The measured corrugation may also be enhanced for probes either more reactive or with larger polarizability such as H or Ne [34–36]. Further investigations should address He GIFAD on other alkali-halide surfaces, aiming to maximize the *intrinsic* corrugation increase.

The authors acknowledge funding from ANPCYT (PICT-2017-1201; PICT-2017-2945) CONICET (PIP 112 201301 00386 CO; PIP 112 201501 00274 CO), and U. N. Cuyo (06/C590).

\*To whom all correspondence should be addressed.  
gisela.bocan@cab.cnea.gov.ar

[1] M. Koini, T. Haber, O. Werzer, S. Berkebile, G. Koller, M. Oehzelt, M. G. Ramsey, and R. Resel, *Thin Solid Films* **517**, 483 (2008).

- [2] A. Patrykiewicz, S. Sokołowski, and K. Binder, *Surf. Sci. Rep.* **37**, 207 (2000).
- [3] A. Schüller, S. Wethekam, and H. Winter, *Phys. Rev. Lett.* **98**, 016103 (2007).
- [4] P. Rousseau, H. Khemliche, A. G. Borisov, and P. Roncin, *Phys. Rev. Lett.* **98**, 016104 (2007).
- [5] A. Schüller, M. Busch, S. Wethekam, and H. Winter, *Phys. Rev. Lett.* **102**, 017602 (2009).
- [6] H. Winter, J. Seifert, D. Blauth, M. Busch, A. Schüller, and S. Wethekam, *Appl. Surf. Sci.* **256**, 365 (2009).
- [7] H. Khemliche, P. Rousseau, P. Roncin, V. H. Etgens, and F. Finocchi, *Appl. Phys. Lett.* **95**, 151901 (2009).
- [8] B. Lalmi, H. Khemliche, A. Momeni, P. Soullisse, and P. Roncin, *J. Phys. Condens. Matter* **24**, 442002 (2012).
- [9] J. Seifert, M. Busch, E. Meyer, and H. Winter, *Phys. Rev. Lett.* **111**, 137601 (2013).
- [10] M. Debiossac, A. Zugarramurdi, H. Khemliche, P. Roncin, A. G. Borisov, A. Momeni, P. Atkinson, M. Eddrief, F. Finocchi, and V. H. Etgens, *Phys. Rev. B* **90**, 155308 (2014).
- [11] J. Seifert and H. Winter, *Phys. Rev. B* **93**, 205417 (2016).
- [12] P. Atkinson, M. Eddrief, V. H. Etgens, H. Khemliche, M. Debiossac, A. Momeni, M. Mulier, B. Lalmi, and P. Roncin, *Appl. Phys. Lett.* **105**, 021602 (2014).
- [13] A. Momeni, E. M. Staicu Casagrande, A. Dechaux, and H. Khemliche, *J. Phys. Chem. Lett.* **9**, 908 (2018).
- [14] H. Winter and A. Schüller, *Prog. Surf. Sci.* **86**, 169 (2011).
- [15] A. Schüller and H. Winter, *Phys. Rev. Lett.* **100**, 097602 (2008).
- [16] A. Schüller, H. Winter, M. S. Gravielle, J. M. Pruneda, and J. E. Miraglia, *Phys. Rev. A* **80**, 062903 (2009).
- [17] A. Momeni, P. Soullisse, P. Rousseau, H. Khemliche, and P. Roncin, *e-J. Surf. Sci. Nanotechnol.* **8**, 101 (2010).
- [18] P. Soullisse, Ph.D. thesis, Orsay, 2011, <https://tel.archives-ouvertes.fr/tel-00625450/>.
- [19] See Supplemental Material at <http://link.aps.org/supplemental/10.1103/PhysRevLett.125.096101> for (i) a set of experimental raw GIFAD patterns and their processing and (ii) vdW PESs information.
- [20] M. S. Gravielle and J. E. Miraglia, *Phys. Rev. A* **90**, 052718 (2014).
- [21] M. S. Gravielle and J. E. Miraglia, *Phys. Rev. A* **92**, 062709 (2015).
- [22] G. A. Bocan and M. S. Gravielle, *Nucl. Instrum. Methods Phys. Res., Sect. B* **421**, 1 (2018).
- [23] L. Frisco, J. E. Miraglia, and M. S. Gravielle, *J. Phys. Condens. Matter* **30**, 405001 (2018).
- [24] A. Schüller, M. Busch, J. Seifert, S. Wethekam, H. Winter, and K. Gärtner, *Phys. Rev. B* **79**, 235425 (2009).
- [25] J. P. Perdew, K. Burke, and M. Ernzerhof, *Phys. Rev. Lett.* **77**, 3865 (1996).
- [26] A. Zugarramurdi and A. G. Borisov, *Phys. Rev. A* **86**, 062903 (2012).
- [27] P. Giannozzi *et al.*, *J. Phys. Condens. Matter* **21**, 395502 (2009).
- [28] R. Sabatini, T. Gorni, and S. de Gironcoli, *Phys. Rev. B* **87**, 041108(R) (2013).
- [29] I. Hamada, *Phys. Rev. B* **89**, 121103(R) (2014).
- [30] M. del Cueto, R. J. Maurer, A. Al Taleb, D. Farías, F. Martín, and C. Díaz, *J. Phys. Condens. Matter* **31**, 135901 (2019).

- [31] U. Specht, M. Busch, J. Seifert, H. Winter, K. Gärtner, R. Włodarczyk, M. Sierka, and J. Sauer, *Nucl. Instrum. Methods Phys. Res., Sect. B* **269**, 799 (2011).
- [32] U. Garibaldi, A. C. Levi, R. Spadacini, and G. E. Tommei, *Surf. Sci.* **48**, 649 (1975).
- [33] M. Debiossac, A. Zugarramurdi, P. Lunca-Popa, A. Momeni, H. Khemliche, A. G. Borisov, and P. Roncin, *Phys. Rev. Lett.* **112**, 023203 (2014).
- [34] D. Farías, H. F. Busnengo, and F. Martín, *J. Phys. Condens. Matter* **19**, 305003 (2007).
- [35] M. S. Gravielle, A. Schüller, H. Winter, and J. E. Miraglia, *Nucl. Instrum. Methods Phys. Res., Sect. B* **269**, 1208 (2011).
- [36] M. Minniti, C. Díaz, J. L. Fernández Cuñado, A. Politano, D. Maccariello, F. Martín, D. Farías, and R. Miranda, *J. Phys. Condens. Matter* **24**, 354002 (2012).